http://dx.doi.org/10.5012/bkcs.2013.34.10.3039

The Dual-frequency (20/40 kHz) Ultrasound Assisted Photocatalysis with the Active Carbon Fiber-loaded Fe^{3+}-TiO_2 as Photocatalyst for Degradation of Organic Dye

Shaofeng Xiong,[†,*] Zhoulan Yin,[†] Yuanjin Zhou,[§] Xianzhong Peng,[§] Wenbin Yan,[‡] Zhixiong Liu,[‡] and Xiangyu Zhang[§]

[†]*School of Chemistry and Chemical Engineering, Central South University, Changsha, Hunan 410083, China*
[*]*E-mail: shfxiong@163.com*
[‡]*College of Chemistry and Chemical Engineering, Jishou University, Jishou, Hunan 416000, P.R. China*
[§]*Xiangda Environmental Protection Co., LTD, Yueyang, Hunan 414400, China*
Received May 27, 2013, Accepted July 23, 2013

Dual-frequency ultrasound assisted photocatalysis (DUAP) method was proposed to degrade a stable organic model effluent, cresol red (CR), using the prepared Fe^{3+}-doped TiO_2 with active carbon fiber loading (Fe^{3+}-TiO_2/ACF) as photocatalyst. The influence of key factors, including Fe doping amount and power density of dual-frequency ultrasounds (20/40 kHz), on the degradation efficiency was investigated. The degradation efficiency rises to 98.7% in 60 min accompanied by the color removal of CR liquid samples from yellow to colorless transparent at optimal conditions. A synergy index of 1.40 was yielded by comparison with single ultrasound assisted photocatalysis (SUAP) and the photocatalysis without ultrasound assisted (UV/TiO_2), indicating that a clear synergistic effect exists for the DUAP process. Obvious enhancement of degradation efficiency for the DUAP process should be attributed to production of large amount of free radicals by strong cavitational effects of dual ultrasounds.

Key Words : Dual-frequency ultrasound, Photocatalysis, Active carbon fiber, Synergistic effect

Introduction

The dye-containing effluent has not only a serious impact on the natural water bodies and land but also the risk of carcinogenicity and teratosis to human being.[1] Therefore, the issues to reduce the toxicity levels to permissible limits prior to its discharge are of critical and vital importance throughout the world. Conventional wastewater treatment processes, such as floatation, coagulation flocculation sedimentation and precipitation, are suitable for stabilization of nonxenobiotic compounds whereas these processes do not work well in dye removal mainly as the result of the low removal efficiency and production of secondary pollution.[2] In recent years, the photocatalysis technique has received considerable attention because of the mild reaction conditions, fast speed and no secondary pollution, *etc*.[3-5] However, the elevation of the degradation efficiency with regard to the opaque or chemically stable organic effluent is still far from satisfaction due to the poor effluent-penetrating ability of UV/Vis light and the limited oxidation ability.[6]

One strategy to solve the problems is the degradation of dye effluent by coupling ultrasonic field with photocatalysis. The penetrating ability of ultrasound is very strong even for the opaque wastewater medium and its penetrating depth can ordinarily attain 15-20 cm.[7,8] Ultrasonic activation also contributes dye degradation via acceleration of the sonolysis of H_2O to form more hydroxide and hydroperoxy radicals that further attack dye organic molecules.[9-12] Some literatures have proposed the single ultrasound assisted photocatalysis which focused on examining the influencing factors, including irradiation time, ultrasonic arrangement and ultrasonic power density, and verifying the synergistic effect.[10-16] However, There is still a urgent need to improve the degradation efficiency with the SUAP process for some chemically stable organic pollutants.[17]

It has been assumed that the dual ultrasounds are capable of exciting more hole-electron pairs by virtue of stronger cavitational effect than that of the single ultrasound. From this viewpoint, we have proposed the dual-frequency ultrasound assisted photocatalysis to degrade organic dyes and verified the significant synergistic effect in the degradation of methylene blue solution.[18] Because data on the DUAP process is scarce and the structure-activity relationship of the TiO_2-based photocatalysts remains unclear, it is necessary to continuously explore its mechanism and testify the feasibility of the DUAP process. In this work, we further degraded cresol red (CR) using the DUAP method with active carbon fiber (ACF)-loaded Fe^{3+}-doped TiO_2 as photocatalyst. Active carbon fiber was introduced to load titania photocatalyst in light of its strong adsorption to the dye molecules. CR was chosen as the target compound because it is one of the representative dangerous dye organics with stable triphenylmethane structure and was used extensively in textile industries for dying nylon, polyacrylonitrile modified nylon, wool, silk and cotton.

Experimental

Materials. Cresol red (CR, AR, Tianjin Kaiyuan Reagent Corporation, China) were used as the target organic pollutants. Fe^{3+}-doped TiO_2 with ACF loading, Fe^{3+}-TiO_2/ACF, is employed as the photocatalyst and prepared with butyl titanate

($Ti(OC_4H_9)_4$) as precursor, $Fe(NO_3)_3{\cdot}9H_2O$ as the iron precursor and ACF as carrier by the sol-gel method.[19] ACF was chosen as carrier because its high adsorption enables the organic pollutants to be concentrated on the surface of the photocatalyst. Other chemicals were obtained as analytical reagents and used without further purification.

Preparation of Photocatalyst Samples. Samples of iron-doped titania with ACF loading (Fe^{3+}-TiO_2/ACF) were prepared by the sol-gel method.[2] In a typical procedure, the step for preparation of sol contains: 17 mL $Ti(OC_4H_9)_4$ was dissolved in 30 mL ethanol with stirring for 30 min to prepare solution A. Different amounts of $Fe(NO_3)_3{\cdot}9H_2O$ (0.01-0.07 mol % of $Ti(OC_4H_9)_4$) were dissolved in a mixture of 5 mL of distilled water, 30 mL of ethanol and 10 mL acetic acid according to the required Fe/Ti molar ratio. Afterward, 0.4 mL of 98% concentrated hydrochloric acid was used as a hydrolysis catalyst to add to the resulting solution, which was herein labeled as solution B. Solution A was added drop wise into the solution B under magnetic stirring at room temperature and hydrolyzed for 60 min to obtain a transparent sol. The ACF-loaded photocatalyst was prepared by aging the resulting sol for 6 h at room temperature and then adding drop-by-drop onto a 6.4 g ACF felt to be adsorbed. Then, it was dried at 353 K in an oven and finally calcined at various temperatures (673-873 K) for 2 h in a nitrogen atmosphere. For convenience, the Fe^{3+}-TiO_2/ACF samples are labeled according to their iron content and calcination temperature, "Fe*T*", where "Fe" referred to the Fe doping amount and "T" referred to the calcined temperature. Taking Fe001T673 as an example, it represents the Fe^{3+}-TiO_2/ACF sample with Fe/Ti = 0.01 mol % calcined at 673 K.

Degradation of CR by Dual-frequency Ultrasound Assisted Photocatalysis. As shown in Figure 1, the reactor consisted of a working volume of 3 ± 0.01 L and allowed circulation of cooling water to maintain the reaction temperature at 20 ± 1 °C. A pyrex beaker containing 1 L CR solution of 10 $mg{\cdot}L^{-1}$ suspended in a temperature controlled bath. The photocatalyst was introduced according to a certain proportion into the beaker. In the case of DUAP, the UV light and the dual ultrasounds irradiated simultaneously. The UV light was offered by a 36-W UV lamp with a maximum irradiation peak at 254 nm that was sleeved in the center of a double-walled quartz cylinder. The dual ultrasound irradiation was produced by a CPS-3 probe type ultrasonic generator (power adjustable, 20 kHz, Shanghai Shengpu Co. Ltd, China) at the upper position and an ultrasonic cleaner in the bottom (100 W, 40 kHz). The former ultrasound generator was connected with the probe type ultrasonic transducer that denoted as transducer-2 and, similarly, the denoted transducer-1 refers to the plate type transducer of the ultrasonic cleaner. By the way, the dual transducers can be arranged at the opposite position or orthogonal position. Air was simultaneously pumped in the CR solution to offer oxygen that provides a sink for photoexcited electrons, forming superoxide $O_2^{\bullet-}$ and hydroperoxide $HO_2^{\bullet-}$. These intermediate species tend to accelerate the separation of the photoexcited hole-electron pairs and thus facilitate the degradation of organic dyes.[20]

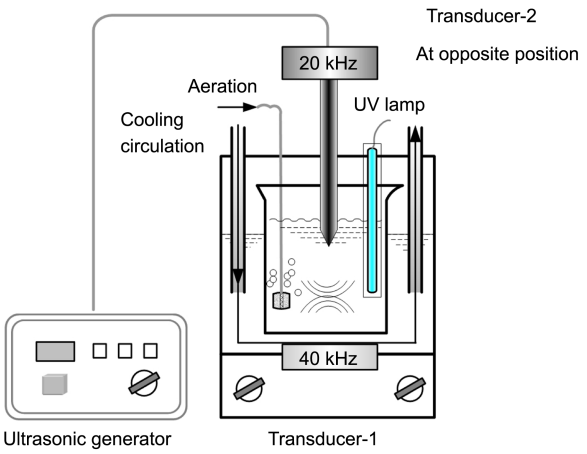

Figure 1. Schematic figure of the dual ultrasound assisted photocatalysis set-up.

In addition, a comparison experiment was designed to obtain the apparent degradation rates of the SUAP and DUAP process for evaluation of the synergistic effect according to a synergy index.[11] For the SUAP process, only the CPS-3 probe type ultrasonic generator or the ultrasonic cleaner was opened and other operational procedures kept invariant as above mentioned.

Analysis Method. The morphology of the Fe^{3+}-TiO_2/ACF photocatalyst was recorded by scanning electron microscope (SEM, JSM-5600LV, JEOL, Japan) at 25 keV. The crystal phases of the TiO_2 particles on ACF support calcined at various temperatures were determined by X-ray diffraction patterns (XRD, D/MAX 2550, Rigaku, Japan) using Cu KR radiation (1.5406 Å) at 40 kV and 100 mA. Ultraviolet-visible spectra of the photocatalysts were recorded using UV–Vis spectrophotometer (Lamda 35, Perkin Elmer instrument) equipped with an integrating sphere. A $BaSO_4$ disc was used as a reference. The scan ranged from 200 to 900 nm. All spectra were monitored in the absorption mode and acquired under ambient conditions. The extent of decoloration for CR solution was assessed by UV-vis spectrophotometry (UV-2450, Shimadzu, Japan). The procedure is as follows: a 10 ml aliquot of the CR solution were pipetted into an amber vial for every 10 min for 50 min and transferred to a quartz cuvette. The change in absorbance was recorded at wavelength of 434 nm. The degradation efficiency (x) of CR at various times was obtained from the efficiency equation: $(C_0-C_t)/C_0 \times 100\%$, where the C_0 is the initial CR concentration ($mg{\cdot}L^{-1}$) and C_t is the CR concentration at time t. All of the reported degradation efficiency values are the average of duplicate experimental results. In addition, the amount of free radicals produced in the DUAP process was also determined spectrophotometrically using methyl blue (MB) as the free radical scavenger. MB undergo the electron-transfer reactions or electrophilic addition reactions with free radicals to form the leuco-methylene blue,[21] which lead to the decline of adsorption peak at 664 nm (A) and discoloration of MB solution. Thus the intensity change of value A is an index to

estimate the free radical amount by an optimum regression equation. In other words, the free radical amount was larger if *A* declined more quickly.

Results and Discussion

SEM Photographs of TiO_2/ACF Photocatalysis. The surface morphologies of the prepared photocatalyst at various temperatures are shown in Figure 2 and it indicates that the TiO_2 coating has been immobilized onto the surface of ACF at a large scale compared to the pristine ACF.

The stress cracks occurred due to thermal shrinkage of the TiO_2 coatings on ACF during calcinations at elevated temperatures from 723 K to 823 K, as shown in Figure 2(b)-(d). The diameters of the original ACF and TiO_2-loaded ACF are respectively 6 ± 1 μm and 7 ± 1 μm, which means that the thickness of the TiO_2 coatings is about 0.5 μm.

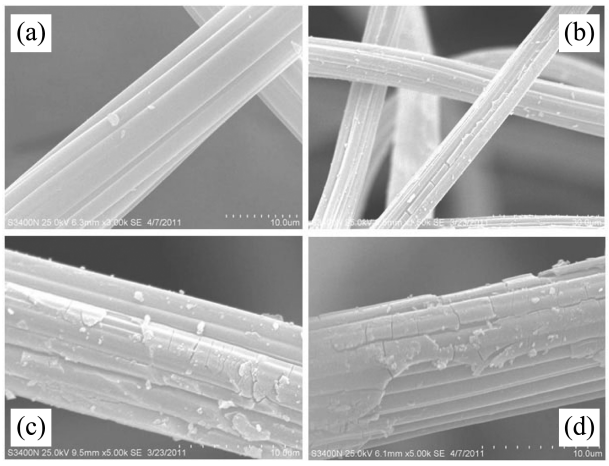

Figure 2. SEM photographs of Fe^{3+}-TiO_2/ACF samples calcined at various temperatures. (a) pristine ACF; (b) Fe^{3+}-TiO_2/ACF calcined at 723 K; (c) Fe^{3+}-TiO_2/ACF calcined at 773 K; (d) Fe^{3+}-TiO_2/ACF calcined at 823 K. Scale bar: 10 μm (a, c, d) and 30 μm (b).

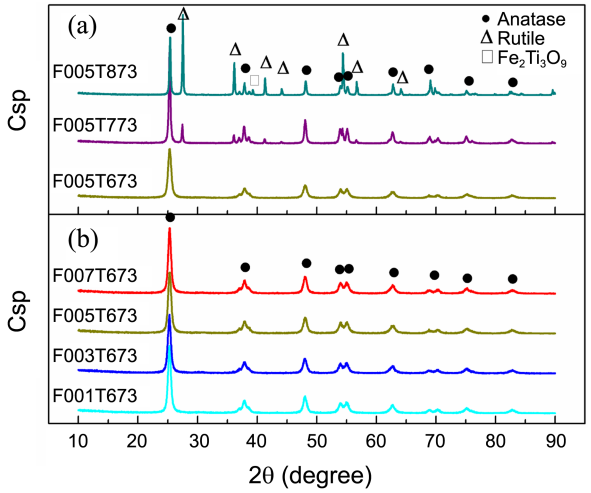

Figure 3. XRD spectrum of Fe^{3+}-doped TiO_2 photocatalyst calcined at various temperatures (a) and with Fe concentra-tion in the range of 0.01-0.07 mol % (b).

X-ray Diffraction Analysis and UV-Vis Absorption Spectra. The Fe^{3+}-doped TiO_2 photocatalyst with Fe concentration in the range of 0.01-0.07 mol % were calcined at 723 K and 773 K for 2 h and then their phases were determined by XRD. As shown in Figure 3(a), several peaks representing the rutile phase of samples Fe005T873 and Fe005T773 were observed and its strength of diffraction became more intense while the strength of diffraction peaks of anatase became weaker. We can identify that anatase phase (JCPDS Card no. 21-1272) start to transform into the rutile phase (JCPDS Card no. 21-1276) at 773 K and rutile phase prevails in proportion at 873 K. As shown in Figure 3b, there is almost no crystalline phase change as the iron dopant concentration increases. Therefore, the iron dopant played a negligible role in affecting the transformation of TiO_2 crystalline phases at a given calcination temperature (673 K) but existed as pseudobrookite ($Fe_2Ti_3O_9$, JCPDS Card no. 40-0850) when the calcination temperature was above 773 K.

UV-Vis Diffuse Reflectance Spectra of Fe^{3+}-TiO_2/ACF Photocatalysts. The UV-Vis diffuse reflectance spectra of Fe^{3+}-TiO_2/ACF photocatalysts doped with various amounts of iron ions are depicted in Figure 4. Undoped TiO_2 has no absorption in the visible region (> 400 nm), whereas Fe^{3+} doped TiO_2 catalysts exhibits both red shifts of the absorption edge and a significant enhancement of light absorption in the range of 400-600 nm. Such absorption increases with increasing the iron content in Fe^{3+} doped TiO_2. Red shift associated with the presence of iron ions can be attributed to a charge transfer transition between the iron ions electrons and the TiO_2 conduction or valence band.

The band gaps of Fe^{3+}-TiO_2/ACF photocatalysts can be estimated with an equation described by Yoneyama *et al.*[22] that plotting $(\alpha h\gamma)^2$ versus $h\gamma$ (inset in Figure 4), where $h\gamma$ is photon energy and α is the absorption coefficient calculated according to the Kubelka-Munk method.[23] The intercept of the tangent to the plot is capable of giving a good approximation of the band gap energy for the fore-mentioned photo-

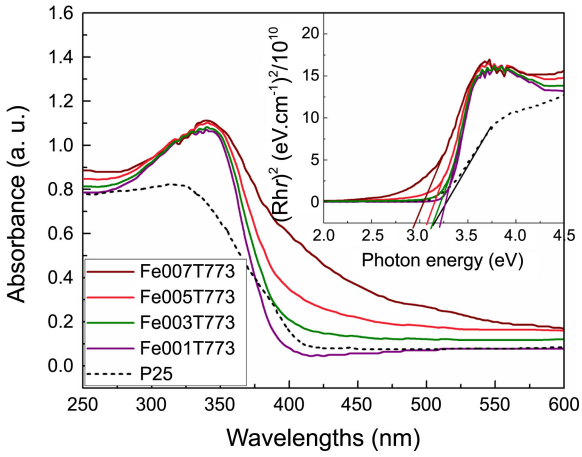

Figure 4. UV-Vis diffuse reflectance spectra of Fe^{3+}-TiO_2/ACF photocatalysts doped with various amounts of iron ions and the corresponding band gap estimated by the intercept of the tangents (Inset).

catalyst.[24] The band gap energies estimated from the intercept of the tangents are 3.22, 3.13, 3.07 and 2.96 eV for the samples Fe001T773, Fe003T773, Fe005T773 and Fe007T773, respectively. The band gap energies are shown to decrease with increasing Fe-doping concentration, which may be caused by a dopant level near the valence band of TiO_2 and the reduction of the band gap of TiO_2.[25] The bandgap of Degussa P25 photocatalyst, a well-known titania photocatalyst composed of anatase and rutile crystallites, was estimated to be 3.15 eV.

Influence of Fe Doping Amount on Photocatalytic Activity. In order to attain the optimal Fe-doping amount and explore its relationship with the catalyst activity, the DUAP process was carried out using the prepared Fe-TiO_2/ACF photocatalysts with Fe-doping amount of 0-0.09 mol % and the results are presented in Figure 5. The photodegradation efficiency in 80 min increased with increasing iron concentration, reaching a inflexion point at 0.07 mol % Fe and the maximum at 0.09 mol % Fe. The activity of Fe-TiO_2/ACF photocatalyst with content of 0.07 mol % Fe is apparently higher than the bare TiO_2 and Degussa P25. It can be attributed to both the decline of band gap energy of Fe-TiO_2/ACF samples (Figure 4) and Fe dopant's role as a trap for the photo-generated electron and the photo-generated hole. For the latter reason, according to Vijayan *et al.*,[26,27] we concluded that Fe dopant (Fe^{3+}) firstly trapped the photogenerated holes to form Fe^{4+} which subsequently migrated to TiO_2 surface and adsorbed hydroxyl ion to produce hydroxyl radicals (OH·). Hydroxyl radical is known as the primary oxidant causing the ultimate self-destruction of CR. However, too high doping level is detrimental to the activity of the photocatalyst due to the blocking core level semiconductor surface by Fe.[28]

Effect of the Ultrasonic Power Density. To investigate the effect of ultrasonic power density on the degradation efficiency in the presence of photocatalysis, the power density of transducer-2 was adjusted in the range of 120-200 W·L^{-1} while the power density of the transducer-1 was kept constant (100 W·L^{-1}). The apparent rate constants were measured with a power interval of 20 W·L^{-1}.

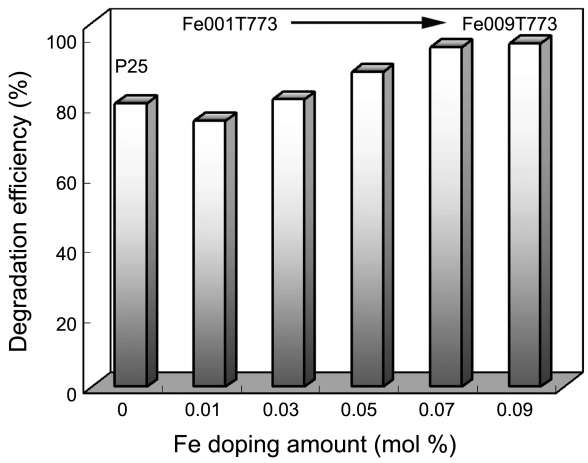

Figure 5. Relationship between Fe-doping amount and the degradation efficiency in the DUAP process.

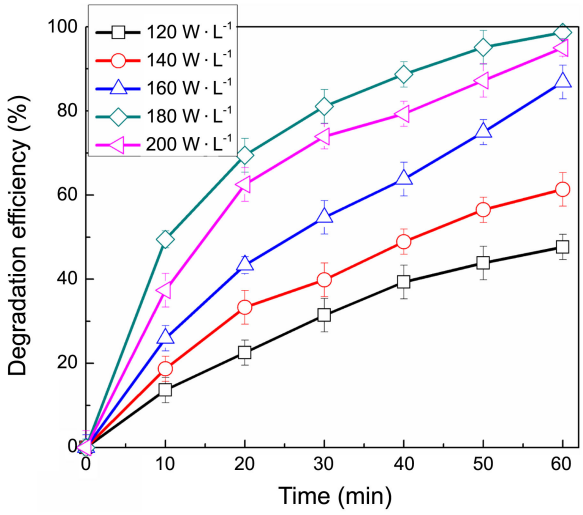

Figure 6. Effect of ultrasonic power density on the degradation efficiency for the DUAP process. Experimental conditions: CR initial concentration C_0=10 mg·L^{-1}, total volume V = 1 L, Fe^{3+}-TiO_2/ACF (Fe007T773), ACF amount C_{ACF} = 120 mg·L^{-1}, natural pH.

The result presented in Figure 6 demonstrates that the increase of ultrasonic power density from 120 W·L^{-1} to 180 W·L^{-1} arouses a significant increase in the degradation efficiency from 41% to 98% in 60 min. It indicates that the improvement of the power density of the ultrasounds favors the CR degradation. Meanwhile, the degradation efficiency in 60 min decreased about 1% as the ultrasonic power density further raised from 180 to 200 W·L^{-1}, meaning that the exorbitant power is technologically and economically unfeasible.

Kinetic Analysis and Evaluation of the Synergistic Effect. To discuss the CR degradation kinetic model and evaluate the synergistic effect of sonophotocatalysis in the DUAP process, the degradation efficiency (x) in various times was analysized under each condition of UV/TiO_2, SUAP and DUAP. The comparison was shown in Figure 7. The power dissipation level for the SUAP with the ultrasonic frequency of 20 kHz and 40 kHz is herein 100 W·L^{-1}. The power dissipation level of DUAP with the ultrasonic transducers arranged in the opposite position is 180 W·L^{-1}.

After a 60 min treatment, the degradation efficiency of CR is respectively 48.7%, 81.7% and 84.7% in the condition of UV/TiO_2, SUAP (20 kHz) and SUAP (40 kHz), whereas the degradation efficiency of CR rises to 98.7% for the DUAP method (opposite). Namely, the combined dual fields can apparently increase the degradation efficiency of CR compared to the photocatalysis with the single ultrasound or without ultrasound assisted.

To further quantitatively describe the degradation rate of CR, the experimental data was fitted to the first-order kinetic expression (Eq. (1)) according to numerous works[29-31]:

$$r_D = \frac{dC}{dt} = \frac{kKC}{1+kC} \quad (1)$$

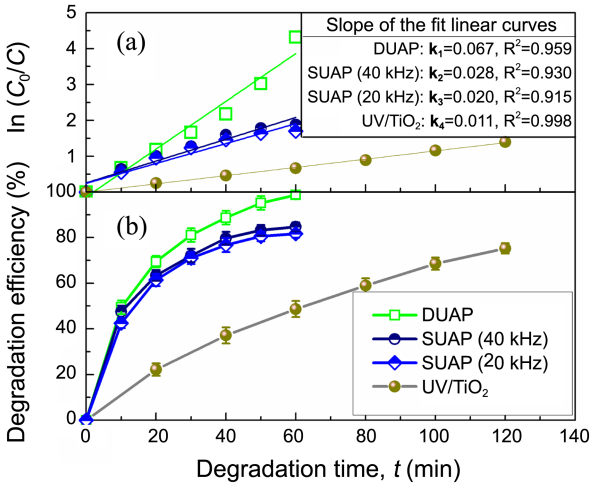

Figure 7. Kinetic analysis of CR Degradation for UV/TiO_2, SUAP and DUAP processes. (a) first-order linear transforms $\mathrm{Ln}C_0/C = f(t)$ of CR degradation. (b) CR degradation efficiency under various conditions. Experimental conditions: CR initial concentration $C_0 = 10$ mg·L^{-1}, total volume $V = 1$ L, Fe^{3+}-TiO_2/ACF (Fe007T773), ACF amount $C_{ACF} = 120$ mg·L^{-1}, natural pH, transducer with 100 W for the SUAP process and 180 W for the DUAP process.

where r_D is the degradation rate of the CR (mg·L^{-1}·min^{-1}), C is the concentration of the reactant (mg·L^{-1}), t is the illumination time, k is the reaction rate constant and K is the adsorption coefficient of the organic dye onto the photocatalyst particles (L·mg^{-1}). When the CR concentration C is micromolar, the value, $1 + kC$, in the denominator can be approximately equal to 1. Thus Eq. (2) can be simplified to an apparent first-order equation:

$$\ln\left(\frac{C_0}{C}\right) = kKt = K_a t \qquad (2)$$

where K_a is the apparent rate constant which can be calculated from the slope of fit linear curves in the Figure 7(a). The results show that the plot of $\ln(C_0/C)$ against time represent approximately linear straight lines, indicating that all the kinetic degradation data of the DUAP, SUAP or UV/TiO_2 process obey the first-order model. Furthermore, the determined K_1 values are 0.067 min^{-1} for the DUAP method, 0.028 min^{-1} for the SUAP process (ultrasonic frequency: 40 kHz), 0.020 min^{-1} for the SUAP process (20 kHz) and 0.011 min^{-1} for the UV/TiO_2 process.

The quantitative way of evaluating any effect (synergistic, additive or negative) for the combining processes is by reference to a synergy index.[11] For the DUAP process, the synergy index is herein defined as $x_{SY} = K_1/(K_2 + K_3)$, where x_{SY} is the synergy index, K_1 is the apparent rate constant of the DUAP process, K_2 is the apparent rate constant of the SUAP process (40 kHz) and K_3 is the apparent rate constant of the SUAP process (20 kHz).

If $x_{SY} > 1$, it indicates that the DUAP process exceeds the sum of the SUAP processes to achieve a synergistic effect on the CR degradation. In the case, substitution of the K values determined in Figure 7(a) for the apparent rate constants in the definition equation yields a synergy index of 1.40, indicating a clear synergistic effect of the DUAP process.

According to Ranjit and Makino *et al.*,[32,33] sonolysis or photocatalysis can produce powerful oxidizing agent like hydroxyl radicals to reduce effluent color and organic load. In view of the significant evaluation of the DUAP degradation efficiency, it may be correlated with large amount of free radicals, which produced by the strong acoustic cavitation of the dual-frequency ultrasound.

On the other hand, to show how much contribute the ultrasound assisted photocatalysis to the degradation reaction of organic dye compared to the ultrasonic-free photocatalysis, a criterion for the difference between the photocatalysis and the ultrasound assisted photocatalysis was similarly proposed by comparison of the reaction rate constant. That is, a ratio of K_{UAP}/K_{UFP} can be used as the criterion for evaluating the contribution degree of ultrasound(s), where K_{UAP} is the reaction rate constant of the ultrasound assisted photocatalysis and K_{UFP} is for the ultrasound-free photocatalysis. If the value of K_{UAP}/K_{UFP} is above 1, it means that the ultrasound facilitates the CR degradation by coupling with the photocatalysis. Furthermore, the larger K_{UAP}/K_{UFP}, the greater contribution the ultrasound(s) make in the ultrasound assisted photocatalysis. The approximation of K_{UAP}/K_{UFP} is 6.09 for DUAP (20/40 kHz), 2.54 for SUAP (40 kHz) and 1.82 for SUAP (20 kHz), respectively. The calculation result indicates that the contribution of the ultrasound(s) in the sonophotocatalysis compared to the ultrasound-free photocatalysis is remarkable, especially for the DUAP process.

The Role of Dual-frequency Ultrasounds in Acceleration of Producing the Free Radicals. As discussed above, it remains unclear whether the acceleration of producing free radicals is caused by the dual-frequency ultrasound in the DUAP process. Further studies are still essential to identify the acoustic cavitation and sonophotocatalytic effect on the amount of free radicals.

UV-vis spectrophotometry is herein chosen as a rapid and precise analytical method to measure the amount of free radicals. The intensity change ratio of the maximum adsorption value (r_A) in the UV-Vis spectrophotometry spectrum correlated with the amount of free radicals can be simply defined by the equation

$$r_A = (A_0 - A_t)/A_0 \times 100\% = \Delta A/A_0 \times 100\% \qquad (3)$$

where A_0, A_t and ΔA are respectively the initial adsorption value, the adsorption value and the adsorption change at time t.

It was shown in Figure 8 that over 98% r_A value could be achieved after only 20 min of treatment of MB solution by the DUAP process but the r_A value for the UV/TiO_2 and SUAP (40 kHz) process dipped to only about 26% and 73%, respectively. As we known, the amount of free radicals produced is proportional to the intensity change ratio of the maximum absorbance peak. Therefore, in contrast to other two advanced treatment methods, the sharp enlargement of free radicals, 98% at 20 min, indicates that the DUAP process offers the apparent physical advantage in activating

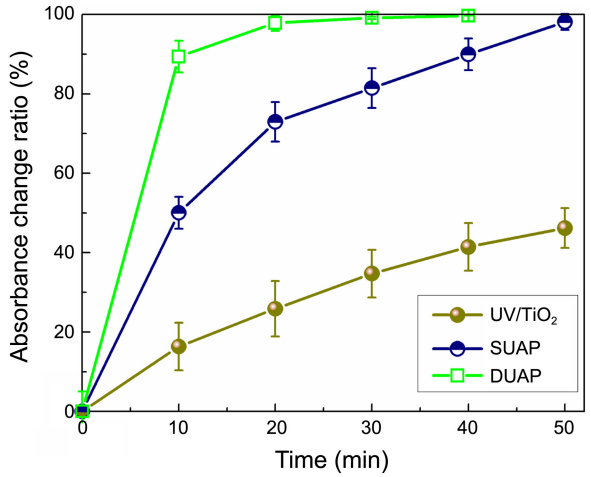

Figure 8. UV-vis spectra of MB solutions for evaluating the amount of free radicals respectively produced in the UV/TiO_2, SUAP and DUAP processes.

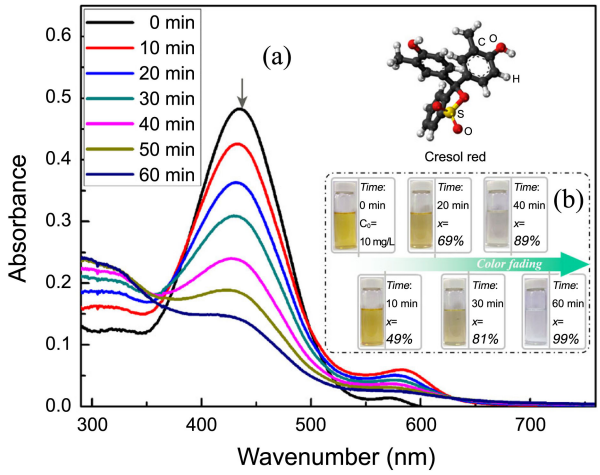

Figure 9. UV-vis spectra of CR solutions (a) and its color removal at various degradation times using the DUAP method (b).

free radicals maybe by the strong acoustic cavitation and the sonophotocatalytic effect.

UV-Vis Absorption Spectra. To obtain better insight into the degradation efficiency, the UV-Vis absorption spectra was employed to identify the change of conjugated chromophore structure of CR in the DUAP process.

Figure 9 shows the variation of UV-Vis absorption spectra of CR in the DUAP process. It can be apparently seen that the absorbance at 434 nm declines continually and nearly disappears at 60 min with a blue-shift of the maximum absorbance peak from 434 to 431 nm. The decline in absorbance at 434 nm indicates that the main conjugated chromophore structure of CR has been destroyed.

Inset b shows the color fading during the course of DUAP. The tendency of the color fading of CR solution is consistent with its UV-Vis spectra.

Conclusion

Cresol red was degraded by the dual-frequency ultrasound assisted photocatalysis method using Fe^{3+}-TiO_2/ACF as the photocatalysis. CR solution with an initial concentration of 10 mg·L^{-1} can be degraded rapidly to 98.7% in 60 min under the experimental conditions of dual ultrasounds at frequency of 20/40 kHz, the power density of 180 W·L^{-1} and Fe^{3+}-TiO_2/ACF photocatalyst concentration of 120 mg·L^{-1}. Based on the experimental data and theoretical analysis of bandgap speculated from the UV-Vis diffuse reflectance spectra, it is shown that the optimal Fe doping content is 0.07 mol % to achieve good activity of Fe-TiO_2/ACF photocatalyst.

The experimental data is consistent with the pseudo-first-order model and a synergy index of 1.40 was yielded indicating a clear synergistic effect of the DUAP method. The acceleration of CR degradation was aroused mainly by strong cavitation effect of ultrasounds that can result in the sonolysis of water to generate large amounts of hydroxyl radical. In addition, it maybe imparts more energy than UV light or single ultrasound to the conduction band of TiO_2 and thus favors transition of electrons and production of the unpaired holes.

Acknowledgments. This research was supported by the Postdoctoral Science Foundation of Central South University and Hunan Provincial Natural Science Foundation of China (No. 12JJ4016). And the publication cost of this paper was supported by the Korean Chemical Society.

References

1. Matsushita, M.; Kuramitz, H.; Tanaka, S. *Environ. Sci. Technol.* **2005**, *39*, 3805.
2. Singh, K.; Arora, S. *Crit. Rev. Env. Sci. Tec.* **2011**, *41*, 807.
3. Agustina, T. E.; Ang, H. M.; Vareek, V. K. *J. Photochem. Photobiolog.* **2005**, 6, 264.
4. Tang, J.; Ye, J. *Chem. Phys. Lett.* **2005**, *410*, 104.
5. Torres, R. A.; Nieto, J. I.; Combet, E.; Pétrier, C.; Pulgarin, C., *Appl. Cata. B* **2008**, *80*, 168.
6. Tong, H.; Ouyang, S.; Bi, Y.; Umezawa, N.; Oshikiri, M.; Ye, J. *Adv. Mater.* **2012**, *24*, 229.
7. Kaur, S.; Singh, V. *Ultrason. Sonochem.* **2007**, *14*, 531.
8. Kılıç, M.; Koçtürk, G.; San, N.; Çınar, Z. *Chemoshphere* **2007**, *69*, 1396.
9. Jin, Y.; Wu, M.; Zhao, G.; Li, M. *Chem. Eng. J.* **2011**, *168*, 1248.
10. Lee, M.; Oh, J. *Ultrason. Sonochem.* **2011**, *18*, 781.
11. Madhavan, J.; Kumar, P. S. S.; Anandan, S.; Zhou, M.; Grieser, F.; Ashokkumar, M. *Chemosphere* **2010**, *80*, 747.
12. Mahamuni, N. N.; Adewuyi, Y. G. *Ultrason. Sonochem.* **2010**, *17*, 990.
13. Mishra, K. P.; Gogate, P. R. *Ultrason. Sonochem.* **2011**, *18*, 739.
14. Neppolian, B.; Ciceri, L.; Bianchi, C. L.; Grieser, F.; Ashokkumar, M. *Ultrason. Sonochem.* **2011**, *18*, 135.
15. Sekiguchi, K.; Sasaki, C.; Sakamoto, K. *Ultrason. Sonochem.* **2011**, *18*, 158.
16. Vajnhandl, S.; Majcen Le Marechal, A. *Dyes Pigments* **2005**, *65*, 89.
17. Zhou, L.; Wang, W.; Zhang, L. *J. Mol. Catal. A-Chem.* **2007**, *268*, 195.
18. Xiong, S. F.; Yin, Z. L.; Yuan, Z. F.; Yan, W. B.; Yang, W. Y.; Liu, J. J.; Zhang, F. *Ultrason. Sonochem.* **2012**, *19*, 756.
19. Shi, J.-W. *Chem. Eng. J.* **2009**, *151*, 241.
20. Pichat, P.; Guillard, C.; Pe, C.; Chopin, T. *Phys. Chem. Chem. Phys.* **1999**, *1*, 4663.

21. Das, N. K.; Mandal, B. M. *Polymer* **1982**, *23*, 1653.
22. Yoneyama, H.; Haga, S.; Yamanaka, S. *J. Phys. Chem.* **1989**, *93*, 4833.
23. Serpone, N.; Lawless, D.; Khairutdinov, R. *J. Phys. Chem.* **1995,** *99*, 16646.
24. Yu, J.; Yu, X. *Environ. Sci. Technol.* **2008**, *42*, 4902.
25. Yamashita, H.; Harada, M.; Misaka, J.; Takeuchi, M.; Ikeue, K.; Anpo, M. *J. Photochem. Photobiol. A* **2002**, *148*, 257.
26. Vijayan, P.; Mahendiran, C.; Suresh, C.; Shanthi, K. *Catal. Today* **2009**, *141*, 220.
27. Zhu, J.; Zheng, W.; He, B.; Zhang, J.; Anpo, M. *J. Mol. Catal. A: Chem.* **2004**, *216*, 35.
28. Ranjit, K. T.; Viswanathan, B. *J. Photochem. Photobiol. A: Chem.* **1997**, *108*, 79.
29. Bertelli, M.; Selli, E. *Appl. Catal. B: Environ*. **2004**, *52*, 205.
30. Visscher, D. A.; Eenoo, P. V.; Drijvers, D.; Langenhove, H. V. *J. Phys. Chem.* **1996**, *100*, 11636.
31. Wang, S.; Gong, Q.; Liang, J. *Ultrason. Sonochem*. **2009**, *16*, 205.
32. Ranjit, K. T.; Willner, I.; Bossmann, S. H.; Braun, A. M. *Environ. Sci. Technol.* **2001**, *35*, 1544.
33. Makino, K.; Mossoba, M. M.; Riesz, P. *J. Am. Chem. Soc.* **1982**, *104*, 3537.